Stability and performance of robust dual-phase (ZrO2)0.89(Y2O3)0.01(Sc2O3)0.10-Al0.02Zn0.98O1.01 oxygen transport membranes

Pirou, Stéven; Bermudez, Jose M. ; Hendriksen, Peter Vang; Kaiser, Andreas; Reina, Tomás Ramirez ; Millan, Marcos ; Kiebach, Wolff-Ragnar

Published in:
Journal of Membrane Science

Link to article, DOI:
10.1016/j.memsci.2017.08.044

Publication date:
2017

Document Version
Peer reviewed version

Stability and performance of robust dual-phase $(ZrO_2)_{0.89}(Y_2O_3)_{0.01}(Sc_2O_3)_{0.10}$-$Al_{0.02}Zn_{0.98}O_{1.01}$ oxygen transport membranes

Stéven Pirou[a], Jose M. Bermudez[b], Peter Vang Hendriksen[a], Andreas Kaiser[a], Tomás Ramirez Reina[b1], Marcos Millan[b], Ragnar Kiebach[a].*

[a] Department of Energy Conversion and Storage, Technical University of Denmark, Risø campus, Frederiksborgvej 399, DK-4000 Roskilde, Denmark

[b] Department of Chemical Engineering, Imperial College London, South Kensington Campus, London SW7 2AZ, United Kingdom

* corresponding author

E-Mail addresses: stepir@dtu.dk, j.bermudez-menendez@imperial.ac.uk, pvhe@dtu.dk, akai@dtu.dk, t.ramirezreina@surrey.ac.uk, marcos.millan@imperial.ac.uk, woki@dtu.dk

[1] T.R.Reina present address: Department of Chemical & Process Engineering, University of Surrey, Guildford, GU2 7HX, United Kingdom

Abstract

Dual phase composite oxygen transport membranes consisting of 50 vol.% $Al_{0.02}Zn_{0.98}O_{1.01}$ and 50 vol.% $(ZrO_2)_{0.89}(Y_2O_3)_{0.01}(Sc_2O_3)_{0.10}$ were successfully developed and tested. The applicability of the membrane in oxy-fuel power plants schemes involving direct exposure to flue gas was evaluated by exposing the membrane to gas streams containing CO_2, SO_2, H_2O and investigating possible reactions between the membrane material and these gases. The analyses of the exposed composites by x-ray diffraction (XRD), x-ray fluorescence (XRF), attenuated total reflection Fourier transform infrared spectroscopy (ATR-FTIR), Raman spectroscopy, and scanning electron microscopy with energy-dispersive X-ray spectroscopy (SEM-EDS) revealed excellent stability. Additionally, an electrical conductivity measurement over 900 h confirmed that the composite is stable under prolonged exposure to CO_2. However, an instability of the dual-phase membrane under oxygen partial pressures below $pO_2 \sim 10^{-4}$ atm. was found. Oxygen permeation tests on a 1 mm thick self-standing membrane resulted in an oxygen flux of 0.33 $mL_N\ min^{-1}\ cm^{-2}$ at 925 °C in air/N_2. Stability tests in CO_2 with 3 vol.% O_2 demonstrated the potential for the use of 10Sc1YSZ-AZO dual-phase membranes in oxy-combustion processes involving direct exposure to flue gas.

Keywords

Oxygen transport membrane, Composite membrane, CO_2 stability, SO_2 tolerance, Oxy-fuel combustion.

Highlights

- 10Sc1YSZ-AZO membranes are stable under oxy-fuel relevant conditions.
- Electrical conductivity of the composite is stable over 900 hours in CO_2.
- Oxygen fluxes-up to 0.33 $mL_N\ min^{-1}\ cm^{-2}$ (925 °C, air/N_2) with 1 mm thick membranes.

1. Introduction

Oxygen transport membranes (OTMs) are a promising technology for producing pure oxygen or supplying oxygen to some oxidation process at both small and large scale. Especially high temperature processes, such as biomass gasification, oxy-fired cement production, or oxy-fuel combustion where some (waste) heat can be made available for air preheating, are interesting application areas. Here, OTMs can provide oxygen at a lower energy consumption than with conventional oxygen production from cryogenic distillation or vacuum pressure swing adsorption, if the OTMs are used in small to medium units and in thermally integrated separation modules [1][2][3].

Typical OTMs are dense membranes made from mixed ionic electronic conductors (MIECs), which enable oxygen diffusion through vacancies in the crystal lattice and simultaneous transport of electrons in the opposite direction. An oxygen partial pressure difference between the gas atmosphere on the feed and the permeate side provides the driving force for the transport of oxygen ions across the membrane. The flux through the membrane is given by the Wagner Equation (1) for the case of fast surface exchange:

$$J_{O_2} = \frac{RT}{16F^2L} \int_{P''_{O_2}}^{P'_{O_2}} \frac{\sigma_e \sigma_i}{\sigma_e + \sigma_i} \, (pO_2) \, d \ln pO_2 \qquad (1)$$

where J_{O_2} is the oxygen permeation flux (mol m^{-2} s^{-1}), R is the gas constant (J mol^{-1} K^{-1}), T is the absolute temperature (K), F is the Faraday constant (A mol^{-1}), L is the membrane thickness (m), σ_e and σ_i are the electronic and the ionic conductivities (S m^{-1}), and P'_{O_2} and P''_{O_2} are the oxygen partial pressures at the high pressure and low pressure sides (Pa), respectively.

In recent years, a significant number of publications have been dedicated to membranes based on single-phase MIEC materials, such as $Ba_{1-x}Sr_xCo_{1-y}Fe_yO_{3-\delta}$ (BSCF) and $La_{1-x}Sr_xCo_{1-y}Fe_yO_{3-\delta}$ (LSCF) [4][5][6][7][8][9][10][11][12]. Their good electronic and ionic conductivities allow high oxygen fluxes. However, most of the promising MIEC materials are not chemically stable under atmospheres containing CO_2 and SO_2,

which is required when using OTMs in “direct integration mode” in biomass gasification, cement production or oxy-combustion based coal fired power plant processes targeting carbon capture. “Direct integration mode” signifies process schemes, where the membranes are exposed directly to a flue gas (or pyrolysis gas) on the permeate side of the membrane. Such direct integration is beneficial for process economy and efficiency but places stringent requirements on the materials, specifically stability in CO_2 and SO_2 which are inevitable constituents/impurities arising from the calcination of limestone, and the combustion of sulfur-containing coal or biomass.

The composition of the flue gas in an oxy-fuel power plant can vary depending on several parameters: oxygen purity, fuel composition and the extent of “false air intrusion”. Therefore, the conditions the membrane is exposed to can vary from case to case. A representative composition would be; CO_2 (80-90 mol.%), N_2 (8-10 mol.%), H_2O (2-3 mol.%), O_2 (2-3 mol.%) and SO_2 (200-500 ppm) [13]. Some of these gases (mainly CO_2 and SO_2) will react quickly with most alkaline-earth doped perovskite based materials (common OTMs materials) leading to reduced permeability due to the formation of alkaline earth carbonates and sulphates such as $(Ba_xSr_{1-x})CO_3$ and $SrSO_4$ [7][14][15][16][17][18][19]. Composite materials of a stable ionic and a stable electronic conductor (in a dual phase membrane) can be an interesting alternative to overcome the stability limitations of single-phase membrane materials in CO_2 and SO_2.

Yttria stabilized zirconia ($(ZrO_2)_{1-x}(Y_2O_3)_x$ (YSZ)) is a well-known strong and stable ionic conductor [20][21][22] which is used in many high temperature applications, such as in SOFC [23][24][25], λ-sensors [26][27][28]. We propose here to develop a stable dual phase membrane based on 10Sc1YSZ as the ionic conductor, because co-doping zirconia with scandium and yttrium ($(ZrO_2)_{1-(x+y)}(Y_2O_3)_x(Sc_2O_3)_y$ (ScYSZ)) significantly increases the ionic conductivity at an operation temperature of 850°C (the ionic conductivity of $(ZrO_2)_{0.92}(Y_2O_3)_{0.08}$ (8YSZ) is 0.03 S cm^{-1} at 850 °C [29] whereas the ionic conductivity for $(ZrO_2)_{0.89}(Y_2O_3)_{0.01}(Sc_2O_3)_{0.10}$ (10Sc1YSZ) is 0.12 S cm^{-1} [30]).

Doped zinc oxide has recently been proposed as an electronic conductor for use in OTMs [31]. There are several reasons for this : (i) The conductivity of ZnO can by doping with small amounts of trivalent elements like Al, Ga or In be raised to more than 100 S/cm (at 820 ºC, $\sigma_{Zn_{0.98}Al_{0.02}O}$=164 S cm^{-1} while σ_{ZnO}=0.016 S cm^{-1}) [32][33][34][35][36][37][38]; (ii) ZnO is chemically stable in both CO_2 and SO_2 atmospheres [31]; and (iii) ZnO is non-toxic, abundant and inexpensive. Accordingly, $Al_{0.02}Zn_{0.98}O_{1.01}$ (AZO) was chosen here as the electronic conductor for the developed dual-phase membrane.

In order to evaluate the possible application of 10Sc1YSZ-AZO membranes in power plant relevant conditions, the stability of the 10Sc1YSZ-AZO composite was studied in different atmospheres, including CO_2, SO_2 and H_2O. Analytical techniques such as X-ray diffraction (XRD), X-ray fluorescence (XRF), attenuated total reflection Fourier transform infrared spectroscopy (ATR-FTIR), Raman spectroscopy and scanning electron microscopy with energy-dispersive X-ray spectroscopy (SEM-EDX) were used to characterize the material after exposure to the gases. Dual-phase membranes were prepared both in the form of thick self-standing membranes (i) and thin asymmetric membranes (ii). The effect of different oxygen partial pressure on the microstructure of the membrane material during sintering and during oxygen permeation tests was investigated. Finally, the performance of the membrane was evaluated by a long-term electrical conductivity measurement under CO_2 and by oxygen permeation tests.

2. Experimental

2.1. Thermochemical stability and characterization of 10Sc1YSZ-AZO composites

2.1.1. Thermochemical stability tests

The thermochemical stability of the 10Sc1YSZ-AZO composite was tested in a quartz up-flow vertical testing unit (Figure 1). This unit consists of a liner containing a porous sample holder to enable an even distribution of gas. The testing unit is fitted inside an oven, capable of operation up to 1200 °C. The temperature is controlled by means of a thermocouple placed within the bed of material.

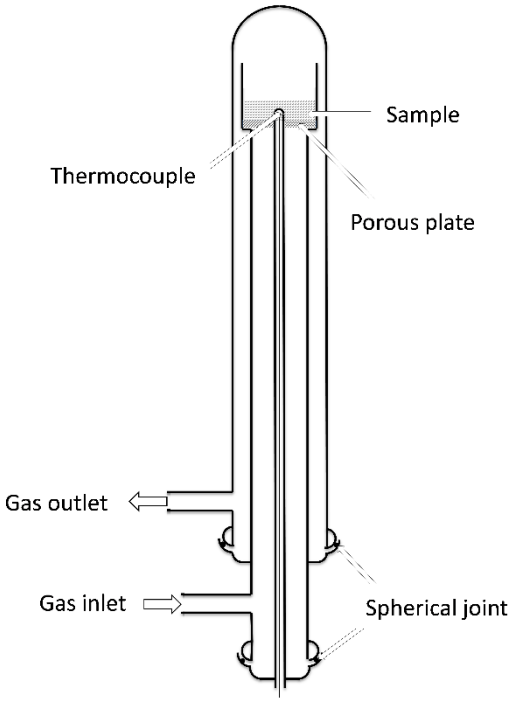

Figure 1: Scheme of the testing unit used for the thermochemical stability tests of the 10Sc1YSZ-AZO samples.

To ensure a large contact area between the gases and the composites, loose powders were used instead of sintered components. For each run, 1 g of fresh 10Sc1YSZ-AZO powder was placed on the sample holder. Then, the testing unit was heated up to 850 ºC in a stationary air atmosphere. At 850 ºC, the gas composition was switched to the desired mixture of CO_2, SO_2 and H_2O to assess the effect of these gases on the stability of the 10Sc1YSZ-AZO. Reference experiments in air and CO_2 were also performed. Different concentrations of CO_2 and SO_2 were provided using two gas cylinders, one with CO_2 (purity 99.8 vol. %) and the other with 2000 ppm of SO_2 in CO_2. Steam was added using an evaporator fed by a syringe pump, which enabled the amount of water to be controlled. The powders were exposed to the different mixtures of $CO_2/SO_2/H_2O$ at a total gas flow rate of 0.25 L_N min^{-1} at atmospheric pressure. The gas compositions used in the different tests are summarized in Table 1. The concentrations of gases in the mixtures were adjusted using flow rotameters. For safety reasons, the outlet gases were cooled down to room temperature to remove steam. Afterwards, the dry flue gases passed through a series of two saturated NaOH solutions to remove SO_2. After the exposure of the powders to the gas atmosphere, the

testing unit was cooled down in the same gas atmosphere to avoid oxygen decomposing the species formed during the treatments and thus recover the material for characterization.

Table 1: Gas compositions in thermochemical stability tests performed on 10Sc1YSZ-AZO powder at 850 °C for 8 hours. A gas flowrate of 0.25 L_N min^{-1} at atmospheric pressure was used.

Test	CO_2 (vol.%) [1]	SO_2 (ppm v/v) [1]	H_2O (vol.%) [2]
Reference[3]	0	0	0
CO_2	100	0	0
$500SO_2$	Balance	500	0
$100SO_2$ $10H_2O$	Balance	100	10
$500SO_2$ $10H_2O$	Balance	500	10
$2000SO_2$ $10H_2O$	Balance	2000	10
$500SO_2$ $30H_2O$	Balance	500	30

[1] Dry basis; [2] Percentage of the total flow, including steam; [3] Performed in air

2.1.2. Material characterization

Before and after the high temperature gas exposure treatment, the powder samples were characterized by a series of analytical techniques to detect any reactions of the powder materials with the different gases.

X-ray diffraction (XRD) patterns were obtained using a PANalytical diffractometer equipped with a Ni-filtered Cu Kα radiation (40 mA, 45 kV) over a 2Θ-range of 5 to 80º and a position-sensitive detector using a step size of 0.05º and a step time of 120 s. The XRD patterns were processed using the X'Pert Highscore Plus software to identify the species present in the samples.

X-ray fluorescence (XRF) was performed to determine the chemical composition of the fresh and treated samples, using a PANalytical Epsilon3XLE X-ray fluorescence spectrophotometer with a 50 kV silver anode tube as source of radiation.

A Perkin Elmer FTIR 100 spectrometer was used to perform attenuated total reflection Fourier transform infrared spectroscopy (ATR-FTIR). Background-subtracted spectra were collected at room temperature and the spectra were baseline-corrected using Spectrum 10™ software.

Raman spectra were collected on a Renishaw InVia Raman spectrometer equipped with a charge-coupled device and a Leica microscope. A 785-nm HPNIR diode laser with maximum power of 300 mW was used as an excitation source. A 1200 mm^{-1} grating was used for all measurements, providing a spectral resolution of ± 1 cm^{-1}. The laser spot was focused on the sample surface using a long working distance 50x. The laser beam spot size was around 1.28 μm.

Scanning electron microscopy with energy-dispersive X-ray spectroscopy studies were done in a JEOL JSM6400 operated at 20 KV and equipped with energy dispersive X-ray spectroscopy (EDS) and wavelength dispersive X-ray spectroscopy (WDS) systems.

2.2. Membrane manufacturing

Thick (1 mm) self-standing symmetric membranes and thin (8 μm) asymmetric supported membranes of 10Sc1YSZ-AZO were prepared (see sections 2.2.1 and 2.2.2) to study the stability of the composite material as a function of the oxygen partial pressure and for oxygen permeation tests.

2.2.1. Thick symmetric membranes

The 10Sc1YSZ and AZO powders were purchased from Daiichi Kigenso Kagaku Kogyo Co. Ldt (Japan) and Nanostructured & Amorphous Material, Inc (USA), respectively. The ionic and electronic conductors were blended in an equal volume ratio to form the 10Sc1YSZ-AZO composite material. The particles size of the powders were adjusted to the submicron range using ball-milling. Subsequently, 15 mm diameter membranes were formed using a uniaxial press (~~90~~ 1 ton load~~MPa~~). The membrane disks were sintered at 1200 °C for 6 hours under different oxygen partial pressures: 0.21 bar (air) and 10^{-5} bar (N_2). After sintering, the sample disks were polished down to 1 mm and an in-house prepared ink of $(La_{0.80}Sr_{0.20})MnO_{3-\delta} - (Y_2O_3)_{0.08}(ZrO_2)_{0.92}$ (LSM-YSZ (50-50 vol.%)) was screen-printed on both sides of the membrane to serve as oxygen oxidation/reduction catalyst. Finally, the membrane was heated to 980 °C for 2 hours in air in order to dry the printed catalyst and make it adhere to the membrane surface.

2.2.2. Thin asymmetric membranes

The asymmetric membranes consist of a 200 µm thick porous support (3YSZ + 20 vol.% of Al_2O_3) and a thin dense composite membrane layer (10Sc1YSZ/AZO, 8 µm) surrounded by two porous layers (8YSZ, 10 µm) which subsequently can be impregnated with a suitable catalyst. All layers were manufactured separately by tape-casting. The YSZ (3YSZ and 8YSZ) powders were purchased from Tosoh (Japan) and were calcined for 2 h at 1100 °C and 900 °C, respectively prior to further processing. All materials were ball milled in ethanol to obtain particles in submicronic range (d_{v50}<1 µm). From these powders three slurries were prepared and used for tape-casting: (i) a slurry for the porous support layer containing 33 wt.% of pore formers in relation to the total solid content (Graphite (d_{v50}=7 µm) and poly(methyl methacrylate) (PMMA) (d_{v50}=1.8 µm) supplied by Graphit Kropfmühl AG (Germany) and Esprix Technologies (USA), respectively) (ii) a slurry for the porous functional layers containing 33 wt.% of pore former (PMMA) and (iii) a slurry for the dense membrane layer free of pore former. The three slurries were prepared using the same organic additives: ethanol (solvent), polyvinylpyrrolidone (PVP, dispersant), polyvinyl butyral (PVB, binder) and polyoxyethylene aryl ether (Pycal 94, plasticiser). After drying, the green tapes were assembled by lamination at 135 °C and 30 mm diameter disks were cut out using a stamping tool. The asymmetric membranes were sintered at 1200 °C for 6 h in different atmospheres in order to study the stability of the thin 10Sc1YSZ-AZO film under various oxygen partial pressures. After sintering, $Gd_{0.2}Ce_{0.8}O_{2-\delta}$ (GDC) and $LaNi_{0.6}Co_{0.4}O_{3-\delta}$ (LNC) aqueous solutions with concentration of 2.5 and 1.25 M were prepared and infiltrated into the YSZ porous layers. The impregnation procedure has been described in detail in a previous study [39].

2.3. Characterization of 10Sc1YSZ-AZO-membranes

10Sc1YSZ-AZO membranes were sintered in different atmospheres in order to study the influence of the oxygen partial pressure on the microstructure of the membranes during the sintering step. The microstructure of the membranes was investigated on polished cross-sections by SEM using a Hitachi TM3000 operated at 15 kV.

Electrical conductivity measurements were performed on a bar (1.7 cm x 0.4 cm x 0.4 cm) of 10Sc1YSZ-AZO (50-50 vol%) prepared by isostatic pressing. The bar was sintered at 1200 °C for 6 h in air prior to the conductivity measurements. The 10Sc1YSZ-AZO bar was heated at 1°C min^{-1} from room temperature to 850 °C and conductivity measured successively in air (24 h), in CO_2 (890 h) and again in air (24 h), to study the impact of the CO_2 on the electrical conductivity of the dual-phase material. The flow of gas was maintained at 100 mL_N min^{-1} by using mass flow controllers (Brooks). An in-house built zirconia-based pO_2 sensor was used to determine the pO_2 in the gases. Current was applied via two strips of platinum (A, B) and the resulting potential was measured between two point probes (C, D). The four terminal resistance, R_{ABCD}, is defined as:

$$R_{ABCD} = \frac{V_{CD}}{I_{AB}} \qquad (2)$$

The electrical conductivity σ, expressed in units of S cm^{-1}, was calculated as below:

$$\sigma = \frac{l}{a \cdot R_{ABCD}} \qquad (3)$$

where a is the cross sectional area of the rod (cm^2) and l is the distance between the potential probes (cm).

Oxygen permeation measurements were conducted in a membrane test rig described previously in [40]. Two permeation tests were performed to evaluate the performances of both the thick self-standing and the thin asymmetric membranes. Two additional tests were done to investigate the stability of the membrane at low oxygen partial pressures. As schematically shown in Figure 2, the membranes were placed in the middle zone of a height adjustable tube furnace, between two alumina tubes. Thermocouples were placed in direct contact with the membrane, inside the alumina tube, in order to monitor the temperature. Tape-cast sodium aluminosilicate (NAS, Na_2O: 17.8 mol%, Al_2O_3: 9.4 mol% and SiO_2: 72.8 mol% [41]) glass rings, with an inner diameter of 9 mm, and a glass transition temperature of 515 °C [40] were used as sealing material between the alumina tubes and the membrane. The exterior surface of the samples were also coated with NAS paste to ensure that oxygen cannot enter from the sweep gas compartment to the membrane. To ensure a gas tight sealing, the membrane was heated

in air up to 940 °C and afterwards cooled to 750 °C. A gas chromatograph was connected to the outlet of the anode side (permeate) to quantify any oxygen leaks into the permeate stream (oxygen that enters the anode compartment via pinholes or insufficient sealing at the membrane periphery). To evaluate the performance of the thick self-standing and thin asymmetric membranes, air (100 $mL_N\ min^{-1}$) and N_2 (150 $mL_N\ min^{-1}$) were fed to the cathode and anode side (feed) of the membrane, respectively. The inlet flow of each gas was controlled and monitored by a mass flow controller (Brooks). In-house built zirconia-based pO_2 sensors were used to determine the pO_2 of the inlet gas on the permeate side (before feeding to the membranes) and of the outlet gas (after passing over the membranes). Oxygen permeation flux was deduced based on the pO_2 variations between the inlet and the outlet of the gas flowing through the anode side. The oxygen permeation flux through the membranes was calculated as:

$$J_{O_2} = \frac{pO_2'' \dot{n}'' - pO_2' \dot{n}'}{A} \qquad (4)$$

where J_{O_2} is the oxygen permeation flux, $pO_2{}'$ and $pO_2{}''$ are respectively the oxygen partial pressures of the inlet and outlet gases, $\dot{n}'$ and $\dot{n}''$ are molar flow rates of inlet and outlet gases, respectively, and A is the net area of the permeate side of the membrane. The Nernst equation (5) is used to calculate the oxygen partial pressure from the measured sensor voltage (V):

$$pO_2 = pO_{2,ref}.e^{\frac{4FV}{RT}} \qquad (5)$$

where V is the open circuit voltage of the oxygen sensor, T is the temperature of the oxygen sensor and $pO_{2,ref}$ is the oxygen partial pressure at the reference electrode which was maintained at 0.21 atm during the measurement.

The stability study of the membrane under low pO_2 atmospheres was carried out on two self-standing membranes of 1 mm thickness at 850 °C. During the first test, a continuous flow of 150 $mL_N\ min^{-1}$ of pure CO_2 was fed to the anode side (sweep), while the second membrane was tested in CO_2 + 3 vol.% of O_2. Both tests were performed using a constant flow of 100 $mL_N\ min^{-1}$ of air as a feed gas. After 200 h, the microstructures of the membranes were analyzed by scanning electron microscopy and compared to a similar fresh membrane.

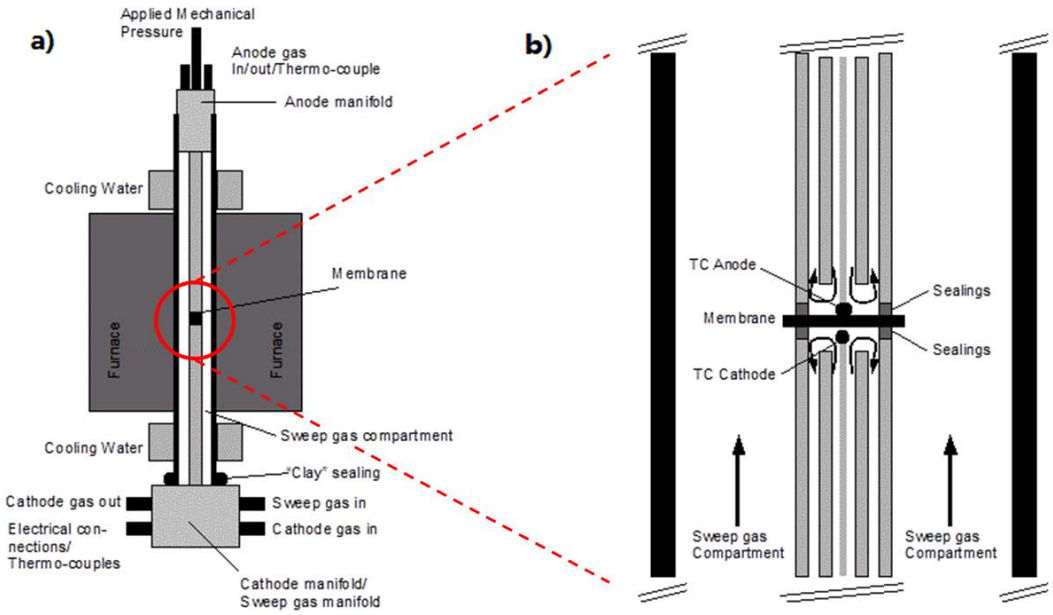

Figure 2: Schematic illustration of the entire membrane test rig used for oxygen permeation measurements, including membrane, furnace, gas supply, manifolds (a) and a zoom into the area with gas compartments, sealings and active membrane (b).

3. Results and discussion

3.1. Stability studies

3.1.1. Chemical stability of 10Sc1YSZ-AZO composite material under relevant flue gas conditions in power plants

Here, the effects of exposure to different impurities in oxy-combustion flue gases, CO_2, SO_2 and H_2O, on the stability of 10Sc1YSZ-AZO powder are presented. In the experiments involving exposure to SO_2, the total amount of sulphur put in contact with the samples was 0.02 g for the experiment using 100 ppm of SO_2, 0.08 g for the experiments with 500 ppm of SO_2, and finally 0.32 g for the experiment using 2000 ppm of SO_2. The relative large quantities of sulfur used in these experiments should improve the detection of any reaction products (sulfates) within the detection limits of the analytical tests.

Figure 3 shows selected results of the XRD characterization before and after exposure of the composite material to CO_2 and SO_2 (plots for further experiments are provided in the Supporting Information, Figure 11). The powder diffractograms of the fresh and the treated samples of 10Sc1YSZ-AZO are identical and additional peaks related to the formation of new crystalline phases could not be observed within the detection limits. The

diffractograms of the fresh and treated samples plotted in Figure 3 correspond to a combination of Sc and Y doped ZrO_2 and $Zn_{0.98}Al_{0.02}O_2$ peaks.

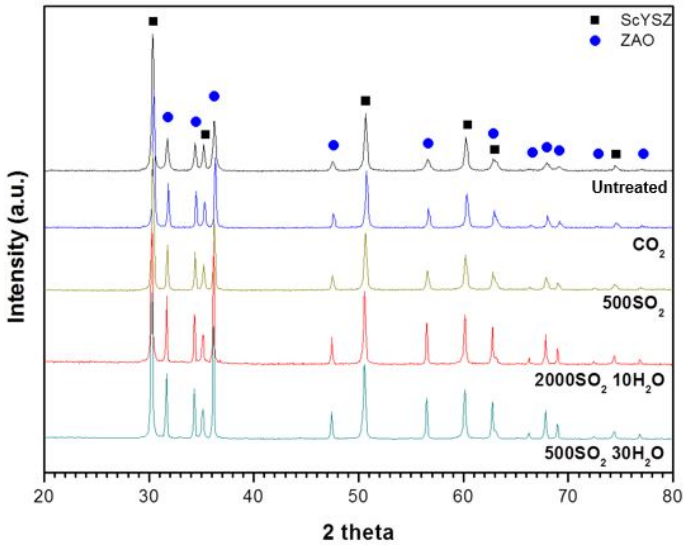

Figure 3: Powder XRD patterns of 10Sc1YSZ-AZO after treatment in different atmospheres (from top to bottom): untreated (black), in pure CO_2 (blue), in a mixture of 500 ppm of SO_2 in CO_2 (yellow), in a mixture of 2000 ppm of SO_2 in CO_2 and 10% of steam (red) and in a mixture of 500 ppm of SO_2 in CO_2 and 30% of steam (cyan).

However, very low amounts of crystalline phases or non-crystalline phases are difficult to detect with powder X-ray diffraction. Therefore, additional characterization by Raman and ATR-FTIR was performed to further exclude any formation of small amounts of secondary phases after exposure to the gases. Figure 4 shows the ATR-FTIR and Raman spectra of the same samples investigated previously by XRD (Figure 3) (more Raman and ATR-FTIR data are included in the Supporting Information Figures 12 and 13). Both techniques are well suited for detection of small amounts of carbonates or sulphates. Any presence of carbonates would be detectable by sharp signals in the range of 850-900 cm^{-1} or broad peaks in the range of 1400-1600 cm^{-1} [42][43][44]. Sulphates would give rise to signals in the range from 950-1250 cm^{-1} [42][43][45] or in the range of 200-800 cm^{-1} and/or between 900 and 1400 cm^{-1} in the Raman spectra. However, it is noteworthy that no new peaks are observed in these ranges when comparing ATR-FTIR and Raman spectra of the samples before and after treatment. The ATR-FTIR and Raman spectra of untreated and treated samples are identical.

With the aim of discarding any possible incorporation of sulphur or carbon during the treatments, also XRF and elemental analysis were performed on the fresh and treated samples. Neither carbon nor sulphur were detected by any of these techniques. It should be noted that the detection limit of these techniques are in the range of a few ppm (if instead alkaline earth containing cobaltite perovskite type materials are investigated after similar exposures with the same characterization techniques significant amounts of both sulphates and carbonates are detected [46]). Finally, SEM images (provided in the Supporting Information, Figure 14) showed that no morphological changes occurred in the samples after the treatment, even in the harshest conditions (2000 ppm of SO_2 in CO_2 + 10% of steam (Figure 14.b), and 500 ppm of SO_2 in CO_2 + 30% of steam (Figure 14.c)). The WDS spectra of these images are also provided. It is possible to see that the signal obtained for the presence of sulphur is lower than the background, thus discarding its presence in the samples.

XRD, XRF, ATR-FTIR, Raman, and SEM-EDS were used to investigate the chemical stability of 10Sc1YSZ-AZO composite material after exposure to gasses characteristic of power plant flue gases. None of the techniques showed presence of any secondary non-desired phases in the treated samples. Accordingly, the analyses prove the excellent stability of the 10Sc1YSZ-AZO composite in the tested environments, indicating that this composite is a good candidate for use in OTMs applied in oxy-combustion processes.

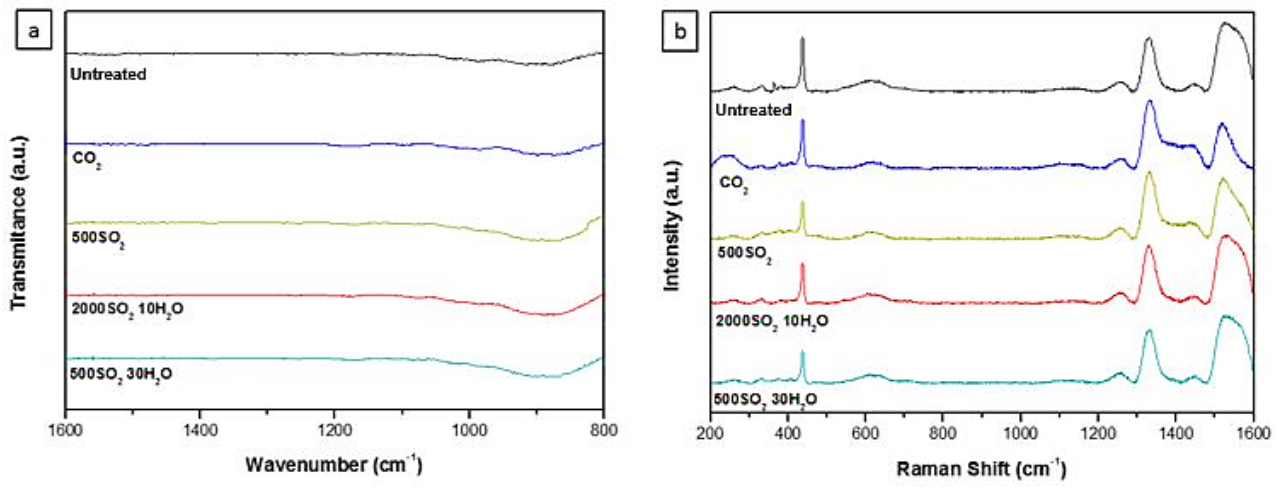

Figure 4: a) ATR-FTIR spectra; and b) Raman spectra of the 10Sc1YSZ-AZO fresh (black), treated with pure CO_2 (blue), with 500 ppm of SO_2 in CO_2 (yellow), with 2000 ppm of SO_2 in CO_2 and 10% of steam (red) and with 500 ppm of SO_2 in CO_2 and 30% of steam (cyan).

3.1.2. Effect of the oxygen partial pressure on the microstructure of 10Sc1YSZ-AZO dual-phase membranes

The effect of the oxygen partial pressure (pO_2) on the microstructure of 10Sc1YSZ-AZO dual-phase membranes during sintering was studied on thick self-standing (1 mm) and thin supported membranes (8 µm).

Figure 5 presents the polished cross-section of 1 mm thick 10Sc1YSZ-AZO membranes after conventional sintering at 1200 °C for 6 h in N_2 (Figure 5.a) and in air (Figure 5.b). The SEM analysis reveals that the membrane sintered in air is completely dense, while the membrane sintered in N_2 is porous on the first 30 µm of each side. The EDS analysis clearly shows the absence of the AZO phase on the sides, while the remaining porous backbone consists of 10Sc1YSZ phase (Figure 5.c). Clearly, a significant amount of AZO is lost when sintering the composite in nitrogen. The microstructure after sintering in N_2 would only be applicable as a membrane if a suitable catalyst is subsequently impregnated into the porous all zirconia structures at the two surfaces. Applying a catalyst on top the membrane surface would not work, as there is no electronic percolation all the way to the sample surfaces. These results are in accordance with results from Bérardan *et al.* [47] which also indicated that AZO was more volatilized during a sintering at high temperature in nitrogen than in air.

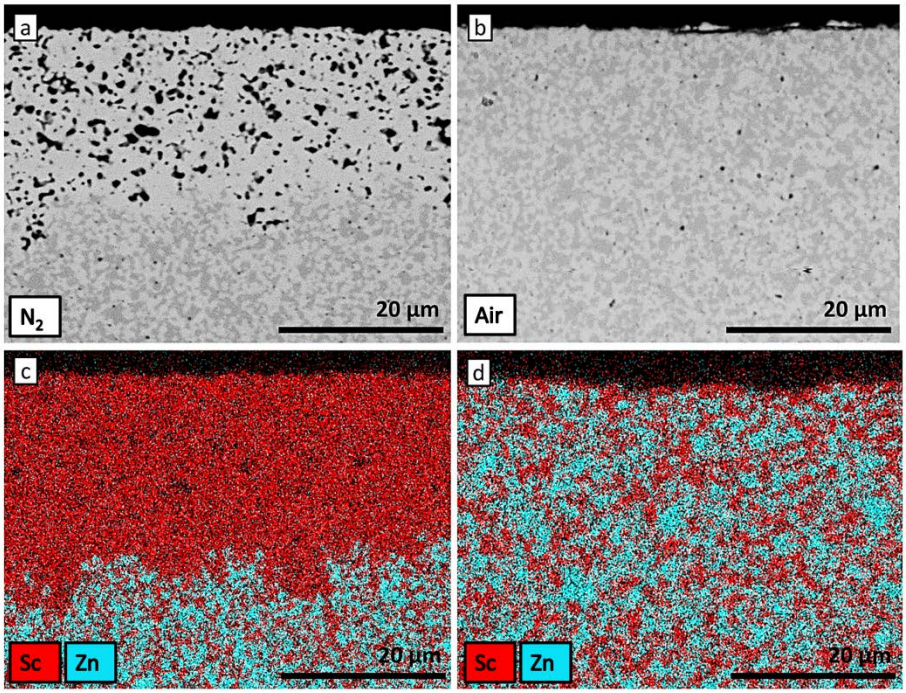

Figure 5: SEM images (top) and EDS maps (bottom) of the elements Sc (red) and Zn (blue) of polished cross-sections of 10Sc1YSZ-AZO membranes, sintered at 1200°C in N_2 (a, c) and in air (b, d)

Figure 6 presents the cross-sections of symmetric membranes composed of a 8 µm thin 10Sc1YSZ-AZO composite layer and a 200 µm 3YSZ support that were sintered at 1200 °C for 6 hours in 3 different atmospheres: (i) N_2, (ii) air and (iii) O_2. Significant alterations of the microstructure in the 10Sc1YSZ-AZO membrane layer can be observed depending on the oxygen partial pressure during the sintering. The membrane sintered in N_2 appears highly porous due to the loose of the zinc oxide phase (Figure 6.a), while under higher oxygen partial pressure atmospheres (air or pure O_2) the composite layer is dense and the desired ratio of ionic/electronic conductor is maintained (Figure 6.b and 6.c).

The study on the membranes microstructure stability shows that the development of 10Sc1YSZ-AZO composite membranes is challenging because of the high volatility of the AZO phase in low oxygen partial pressure atmospheres. When using thick self-standing membranes, this problem can easily be circumvented by removing the 10Sc1YSZ porous phase on both sides of the membranes by polishing. The same issue cannot be so

simply solved with thin asymmetric membranes. Therefore, for the development of asymmetric membrane, sintering has to be performed under sufficiently high oxygen partial pressure in order to keep the AZO phase in the composite. This is not easily achieved as even when applying pure oxygen during sintering a thin dense layer without much ZnO forms at the interfaces between the dense layer and the infiltration layers (see Fig. 6 b and c). This layer will hamper membrane performance, as there is no electronic percolation through this layer.

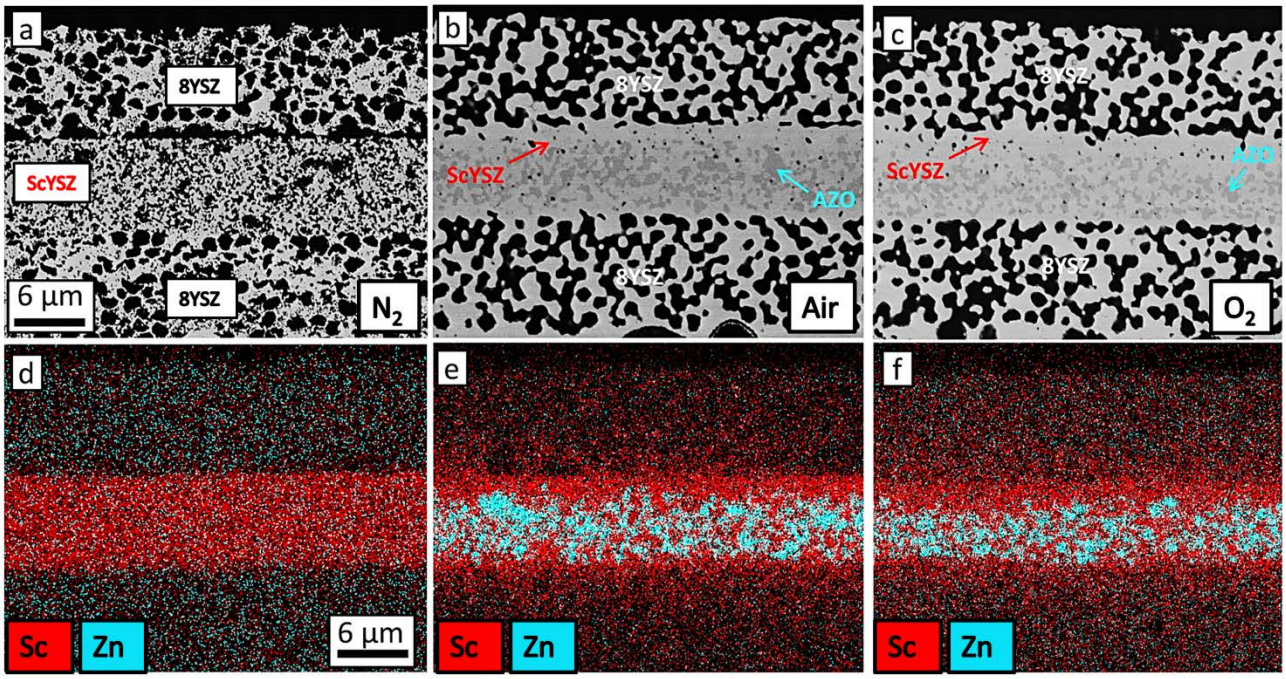

Figure 6: SEM images and EDS maps (Sc and Zn elements) of 10Sc1YSZ-AZO (50-50 vol.%) thin asymmetric membranes sintered at 1200°C in N_2 (a, d), air (b, e) and pure oxygen (c, f).

3.2. Electrical conductivity measurements

As briefly introduced in section 2.3, a long-term electrical conductivity test was performed on a 10Sc1YSZ-AZO composite bar at 850 °C in CO_2 in order to investigate the influence of a prolonged exposure to CO_2 on the electrical conductivity of the dual-phase material. Figure 7 presents the electrical conductivity of the composite material and the oxygen partial pressure realised during the test as a function of time. Initially air was fed to the furnace and after 24 h, the feed was changed to CO_2. After 890 h in CO_2 air was again applied for 24 h. Overall, the electrical conductivity did not decrease during the 900 h of testing. The conductivity increases by a factor of 10 when switching from air to CO_2 showing the expected increase of the electrical conductivity of AZO by

lowering the pO_2 [47][48]. The first and last 24 h of the test, performed in air, gave similar values of conductivity (4% of derivation), thus indicating that the initial electrical conductivity of the composite material (in air) can be recovered. In other words, changes in the conductivity of the samples were not observed when switching back to air atmosphere after treatment in CO_2 and any changes in conductivity are due to the defect-chemistry of AZO (that responds reversibly to pO_2 changes) and not effects of microstructural changes.

The cross-sections of the 10Sc1YSZ-AZO composite bar after the electrical conductivity measurement are shown in Figure 8. Figure 8.a displays the microstructure of a sample section where the platinum paste was applied locally as a current collector covering the sample surface, while Figure 8.b shows a section not covered by the platinum. The comparison of the two images clearly shows that the Pt layer supresses the volatilization of the AZO. Consequently, the current feed probes applied during conductivity measurements seems to have worked well, i.e. contact is not lost here despite the tendency of the sample to lose AZO. The effective conductivity of the bar would be expected to drop a little over time as clearly the top ~4 microns of sample have become depleted in the electronic conductor. However, as the depleted layer constitutes only a small fraction of the cross section the effect of the depletion is not observed over the period in CO_2. After returning to air, indeed a small reduction in the sample conductance is observed which could in part be due to loss of AZO. The conductivity measurements presented in Figure 7 show that the exposure to CO_2 (and associated reduction in oxygen activity) itself increases the sample conductivity. XRD patterns, ATR-FTIR and Raman spectra, in Figures 3 and 4 show that CO_2 does not react or directly contributes to the destabilization of AZO. Nevertheless, the loss of AZO in the dual phase material (Figure 8.b) over time will lead to a decrease of the conductivity because of the loss of the electrical conducting phase. It is important to note here that the conductivity test was performed in much lower oxygen partial pressure ($pO_2 \approx 2.10^{-4}$ bar) than at realistic conditions of the envisioned application areas ($pO_2 \approx 3.10^{-2}$ bar [13]). It is essential to distinguish between the effect of the CO_2 and the effect of the low oxygen partial pressure, when discussing the stability of the composite. This is further investigated and discussed below in section 3.3.2.

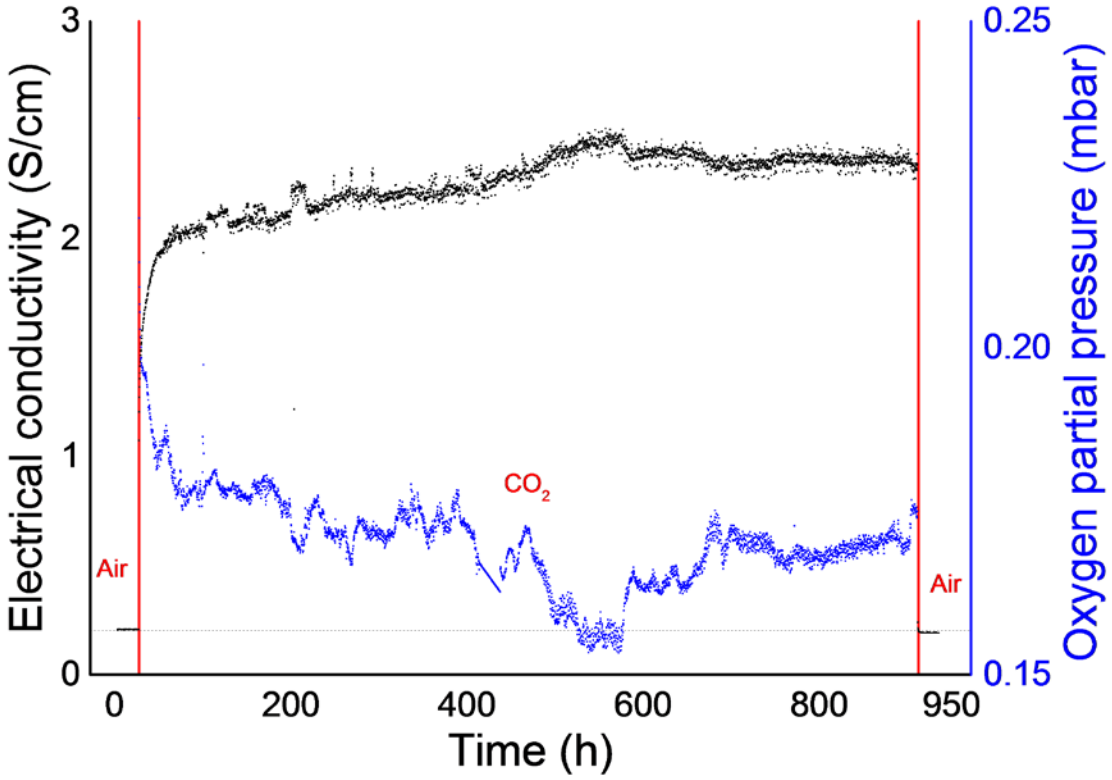

Figure 7: Electrical conductivity of a 10Sc1YSZ-AZO bar (black curve) and oxygen partial pressure in the platform test (blue curve) as a function of the time. The test was performed at 850°C in air (first and last 24 h) and in CO_2. The dotted line represents the initial value of the electrical conductivity in air.

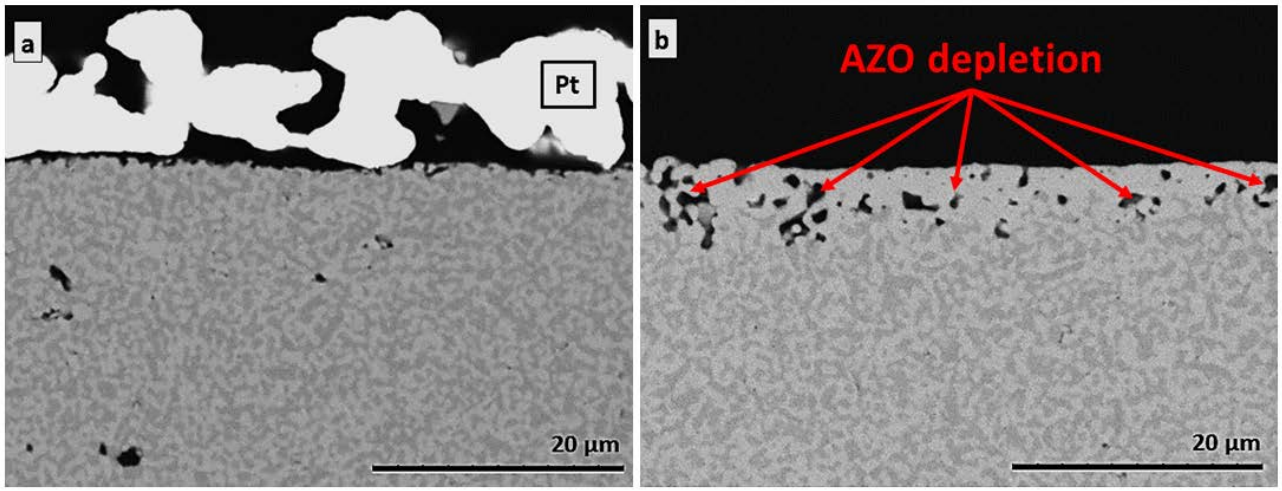

Figure 8: SEM images of polished cross-sections of the 10Sc1YSZ-AZO bar after the electrical conductivity measurement with (a) and without (b) Pt current collector.

3.3. Oxygen permeation measurements

3.3.1. Performances of thick self-standing and thin supported membranes

The performance of a 1 mm thick 10Sc1YSZ-AZO self-standing membrane and an 8 µm thick 10Sc1YSZ-AZO supported membrane was evaluated carrying out oxygen permeation measurements, as described in Section 2.3.

Figure 9 presents the oxygen permeation fluxes of the two membranes with different thicknesses as a function of temperature when using N_2 as sweep gas, and air as a feed gas. Based on the Wagner equation (1), described in section 1, the oxygen flux should scale inversely with membrane thickness. Interestingly, the opposite was found here: the 1 mm thick membrane shows a higher oxygen flux than the thin asymmetric membrane. As shown in Figure 9, at 925 °C the oxygen flux through the 1 mm thick membrane corresponds to 0.33 $mL_N\ min^{-1}\ cm^{-2}$, while only a flow of 0.16 $mL_N\ min^{-1}\ cm^{-2}$ was measured across the thin supported membrane. Clearly, the performance of the asymmetric membrane is drastically lower than anticipated. Considering that the asymmetric membrane is approximately a hundred times thinner than the self-standing membrane and that the oxygen permeation flux through the self-standing membrane is mainly limited by the bulk diffusion, a significant increase of the oxygen permeation flux would be expected when using the thin asymmetric membrane. A likely explanation for the low performance is a lack of percolation in the electronic phase across the dense 10Sc1YSZ-AZO composite layer. The SEM micrographs of the cross sections (Figure 6.b) shows clear signs that the outer parts of the dense membrane layer are completely depleted in AZO and would behave effectively as an electrolyte hampering the oxygen permeation flux.

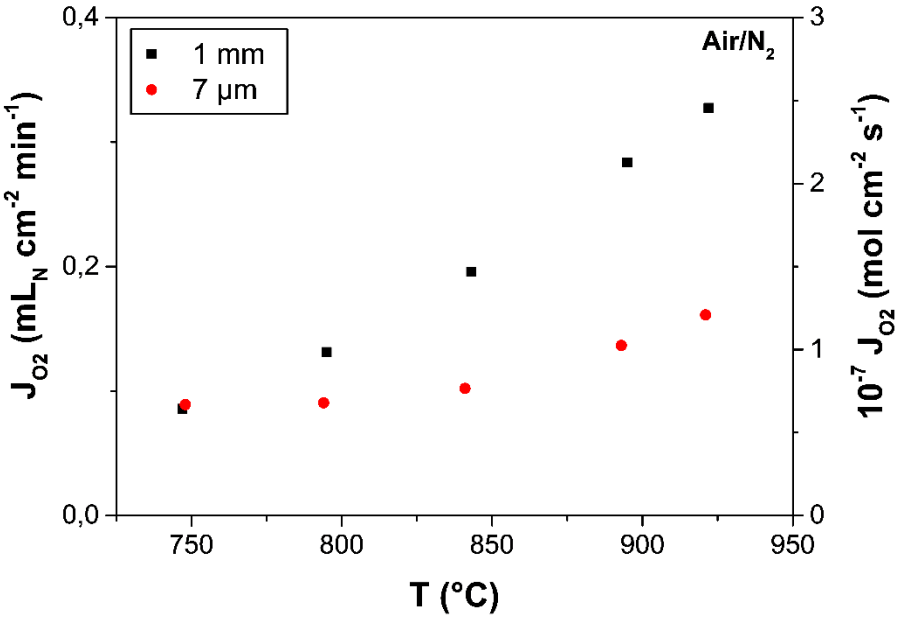

Figure 9: Oxygen permeation fluxes of 10Sc1YSZ-AZO membranes as a function of the temperature using air as a feed gas and N_2 as a sweep gas.

3.3.2. Long-term stability tests in CO_2

To further investigate the influence of the pO_2 on the microstructural degradation of the membrane and to confirm that the observed instability of AZO is due to the mildly reducing atmosphere (pO_2 <10^{-4} bar) and not of the presence of CO_2, the stability of 1 mm thick self-standing membranes was investigated under different pO_2 conditions on the sweep side. One membrane was tested under an air/CO_2 gradient while the other test was conducted between air and CO_2 + 3 vol.% of O_2. It should be emphasized that the pO_2 conditions of the second test resembles realistic conditions for an application of the OTMs in oxy-fuel power plants [13], and are therefore considered the more relevant. After 200 h of exposure, the microstructure of the tested membranes was compared to a fresh membrane. Results are presented in Figure 10. The polished cross-section of a fresh membrane is displayed in Figure 10.a, the membrane tested with pure CO_2 on the permeate side is presented in Figure 10.b and finally the membrane tested in CO_2 + 3 vol.% O_2 is reproduced in Figure 10.c. As expected, from both the long term conductivity test and the studies of the sintering in various gasses, a significant loss of AZO is observed for the membrane exposed to pure CO_2 after 200 hours due to the instability of the AZO phase in low pO_2 atmosphere ($pO_2 \approx 2.10^{-4}$ bar). The first 10 µm on the sweep side appear highly porous. However, the microstructure of the

second long term tested membrane is practically identical to the fresh one, demonstrating that no AZO is lost under exposure to CO_2 with 3 vol.% of O_2 at the sweep side . This experiment proves that the 10Sc1YSZ-AZO dual-phase membranes is applicable under oxy-fuel conditions (high CO_2 activity) as long as the oxygen activity at the permeate side is maintained at ~2-3 %. For the case of a low pO_2 ~10^{-4} atm. the membrane would, if in the form of a thin film, most likely not be applicable due to the observed loss of material.

A previous study from Cheng *et al.* reported on the use of AZO in a composite oxygen membrane in combination with CGO [31]. A stable flux through a 1 mm thick membrane over ~500 hours in a gradient between air and CO_2 was also found elucidating material robustness towards CO_2. However, the conducted thick membrane experiment [31]"masks" problems related to material loss under low pO_2 as discussed here for AZO/zirconia composites due to the large material reservoir. Given the material loss rates observed here, it is unlikely that any thin film (L~10-20 micron) composite membrane realization involving AZO would perform reliably under long term operation (thousands of hours) if the pO_2 on the permeate side is lower than 10^{-4} bar. If pO_2 on the permeate side is on the order of 10^{-2} bar material loss seems tolerable (c.f. Figure 10.c).

Practical application of the investigated composite would require the flux can be increased substantially above the values reported in Figure 9. The obvious approach, as also adopted here, would be to reduce the membrane thickness. Whereas a thin film component strong enough for test could obviously be manufactured, it presented no gain in oxygen transport (see section 3.3.1.). This, as discussed (section 3.3.1.) is most likely due to thin "all electrolyte" skin layers that form during firing of the component due to loss of AZO from the surface of the composite. Hence, it is related to the high vapor phase of the ZnO and its limited stability under reducing conditions. Countering measures must be developed to prevent this surface depletion if the full potential of ZnO as a cheap electronic conductor in composite oxygen membranes should be realized. A stabilization of the zinc oxide phase could be achieved by decreasing the sintering temperature, for example by using a dopant element as a sintering aid. The utilization of a protective porous layer with a high AZO content covering the dense membrane would help to prevent the depletion of the zinc oxide phase and seems a feasible route to reduce the problem.

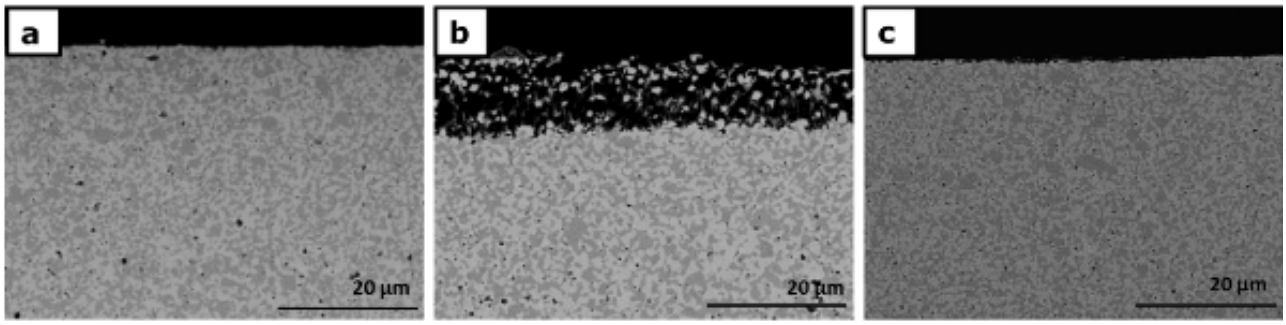

Figure 10: SEM images of the polish cross-sections of 1 mm thick self-standing 10Sc1YSZ-AZO membranes. (a) fresh membrane, (b) tested in air/CO_2 atmosphere, and (c) tested in air/CO_2 + 3 vol.% O_2 atmosphere.

4. Conclusions

The stability of the dual-phase composite membranes consisting of 50 vol.% $Al_{0.02}Zn_{0.98}O_{1.01}$ (AZO) and 50 vol.% $(ZrO_2)_{0.89}(Y_2O_3)_{0.01}(Sc_2O_3)_{0.10}$ (10Sc1YSZ) was studied in simulated oxy-fuel power plant flue gas atmospheres (CO_2, SO_2, H_2O) using several characterization techniques (XRD, XRF, ATR-FTIR, Raman and SEM-EDX). The tests underlined the excellent stability of the materials under application relevant atmospheres. 10Sc1YSZ-AZO is concluded to be a promising material combination for OTMs integrated in oxy-fuel power plants where oxygen activity on the permeate side is above 2.10^{-4} atm. The material is not suitable for use in gasification applications or other applications where the oxygen content on the permeate side is below 100 ppm. In addition the low stability of the zinc oxides phase under very mildly reducing atmosphere makes the fabrication of thin and high performance asymmetric membranes complicated (due to formation of all electrolyte "skin layers"). Clearly thick self-standing membranes show too limited performances to be commercialized and further R&D is required to realize thin and highly performing 10Sc1YSZ-AZO asymmetric membranes, where performance is not limited by lack of electronic percolation, as was the case for the here tested asymmetric membranes.

Acknowledgments

The financial support from EU through the “Graded Membranes for Energy Efficient New Generation Carbon Capture Process (GREEN-CC)” project (Grant agreement no. 608524) is gratefully acknowledged. Henrik Paulsen is acknowledged by the authors for helping with the preparation of the samples for SEM-EDX analysis.

References

[1] S.S. Hashim, A.R. Mohamed, S. Bhatia, Oxygen separation from air using ceramic-based membrane technology for sustainable fuel production and power generation, Renew. Sustain. Energy Rev. 15 (2011) 1284–1293. doi:10.1016/j.rser.2010.10.002.

[2] M. Puig-Arnavat, S. Soprani, M. Søgaard, K. Engelbrecht, J. Ahrenfeldt, U.B. Henriksen, P.V. Hendriksen, Integration of mixed conducting membranes in an oxygen–steam biomass gasification process, RSC Adv. 3 (2013) 20843–20854. doi:10.1039/c3ra44509g.

[3] M. Czyperek, P. Zapp, H.J.M. Bouwmeester, M. Modigell, K. Ebert, I. Voigt, W.A. Meulenberg, L. Singheiser, D. Stöver, Gas separation membranes for zero-emission fossil power plants: MEM-BRAIN, J. Memb. Sci. 359 (2010) 149–159. doi:10.1016/j.memsci.2010.04.012.

[4] R. Kiebach, K. Engelbrecht, K. Kwok, S. Molin, M. Søgaard, P. Niehoff, F. Schulze-Küppers, R. Kriegel, J. Kluge, P.V. Hendriksen, Joining of ceramic $Ba_{0.5}Sr_{0.5}Co_{0.8}Fe_{0.2}O_3$ membranes for oxygen production to high temperature alloys, J. Memb. Sci. 506 (2016) 11–21. doi:10.1016/j.memsci.2016.01.050.

[5] S. Baumann, J.M. Serra, M.P. Lobera, S. Escolástico, F. Schulze-Küppers, W.A. Meulenberg, Ultrahigh oxygen permeation flux through supported $Ba_{0.5}Sr_{0.5}Co_{0.8}Fe_{0.2}O_{3-\delta}$ membranes, J. Memb. Sci. 377 (2011) 198–205. doi:10.1016/j.memsci.2011.04.050.

[6] P. Haworth, S. Smart, J. Glasscock, J.C. Diniz da Costa, High performance yttrium-doped BSCF hollow fibre membranes, Sep. Purif. Technol. 94 (2012) 16–22. doi:10.1016/j.seppur.2012.04.005.

[7] M. Arnold, H. Wang, A. Feldhoff, Influence of CO_2 on the oxygen permeation performance and the microstructure of perovskite-type $(Ba_{0.5}Sr_{0.5})(Co_{0.8}Fe_{0.2})O_{3-\delta}$ membranes, J. Memb. Sci. 293 (2007) 44–52. doi:10.1016/j.memsci.2007.01.032.

[8] Z. Shao, W. Yang, Y. Cong, H. Dong, J. Tong, G. Xiong, Investigation of the permeation behavior and stability of a $Ba_{0.5}Sr_{0.5}Co_{0.8}Fe_{0.2}O_{(3-\delta)}$ oxygen membrane, J. Memb. Sci. 172 (2000) 177–188. doi:10.1016/S0376-7388(00)00337-9.

[9] L. Ge, W. Zhou, R. Ran, S. Liu, Z. Shao, W. Jin, N. Xu, Properties and performance of A-site deficient $(Ba_{0.5}Sr_{0.5})_{1-x}Co_{0.8}Fe_{0.2}O_{3-\delta}$ for oxygen permeating membrane, J. Memb. Sci. 306 (2007) 318–328. doi:10.1016/j.memsci.2007.09.004.

[10] Z. Taheri, K. Nazari, N. Seyed-Matin, A.A. Safekordi, B. Ghanbari, S. Zarrinpashne, R. Ahmadi, Comparison of oxygen permeation through some perovskite membranes synthesized with EDTNAD, React. Kinet. Mech. Catal. 100 (2010) 459–469. doi:10.1007/s11144-010-0158-2.

[11] F. Schulze-Küppers, S. Baumann, F. Tietz, H.J.M. Bouwmeester, W.A. Meulenberg, Towards the fabrication of $La_{0.98-x}Sr_xCo_{0.2}Fe_{0.8}O_{3-\delta}$ perovskite-type oxygen transport membranes, J. Eur. Ceram. Soc. 34 (2014) 3741–3748. doi:10.1016/j.jeurceramsoc.2014.06.012.

[12] X. Tan, Z. Wang, B. Meng, X. Meng, K. Li, Pilot-scale production of oxygen from air using perovskite hollow fibre membranes, J. Memb. Sci. 352 (2010) 189–196. doi:10.1016/j.memsci.2010.02.015.

[13] E.S. Rubin, A.B. Rao, M.B. Berkenpas, Technical Documentation: Oxygen-based Combustion Systems (Oxyfuels) with Carbon Capture and Storage (CCS), 2007.

[14] X. Tan, N. Liu, B. Meng, J. Sunarso, K. Zhang, S. Liu, Oxygen permeation behavior of $La_{0.6}Sr_{0.4}Co_{0.8}Fe_{0.2}O_3$ hollow fibre membranes with highly concentrated CO_2 exposure, J. Memb. Sci. 389 (2012) 216–222. doi:10.1016/j.memsci.2011.10.032.

[15] S. Engels, T. Markus, M. Modigell, L. Singheiser, Oxygen permeation and stability investigations on MIEC membrane materials under operating conditions for power plant processes, J. Memb. Sci. 370 (2011) 58–69. doi:10.1016/j.memsci.2010.12.021.

[16] J. Gao, L. Li, Z. Yin, J. Zhang, S. Lu, X. Tan, Poisoning effect of SO_2 on the oxygen permeation behavior of $La_{0.6}Sr_{0.4}Co_{0.2}Fe_{0.8}O_{3-\delta}$ perovskite hollow fiber membranes, J. Memb. Sci. 455 (2014) 341–348. doi:10.1016/j.memsci.2013.12.073.

[17] E. Bucher, A. Egger, G.B. Caraman, W. Sitte, Stability of the SOFC Cathode Material $(Ba,Sr)(Co,Fe)O_{3-\delta}$ in CO_2-Containing Atmospheres, J. Electrochem. Soc. 155 (2008) B1218. doi:10.1149/1.2981024.

[18] S.J. Benson, D. Waller, J.A. Kilner, Degradation of $La_{0.6}Sr_{0.4}Fe_{0.8}Co_{0.2}O_{3-\delta}$ in Carbon Dioxide and, J. Electrochem. Soc. 146 (2000) 1305–1309.

[19] M. Schulz, R. Kriegel, A. Kämpfer, Assessment of CO_2 stability and oxygen flux of oxygen permeable membranes, J. Memb. Sci. 378 (2011) 10–17. doi:10.1016/j.memsci.2011.02.037.

[20] S. Lia, W. Jin, N. Xu, J. Shi, Mechanical strength, and oxygen and electronic transport properties of $SrCo_{0.4}Fe_{0.6}O_{3-\delta}$-YSZ membranes, J. Memb. Sci. 186 (2001) 195–204.

[21] B. Wang, M. Zhan, D. Zhu, W. Liu, C. Chen, Oxygen permeation and stability of $Zr_{0.8}Y_{0.2}O_{0.9}$–$La_{0.8}Sr_{0.2}CrO_{3-\delta}$ dual-phase composite, J. Solid State Electrochem. 10 (2006) 625–628. doi:10.1007/s10008-006-0136-9.

[22] M.M. Hiroaki Yanagida, Kunihiko Koumoto, Kunihito Komoto, The Chemistry of Ceramics, 1996.

[23] M. Han, X. Tang, H. Yin, S. Peng, Fabrication, microstructure and properties of a YSZ electrolyte for SOFCs, J. Power Sources. 165 (2007) 757–763. doi:10.1016/j.jpowsour.2006.11.054.

[24] C.-J. Li, C.-X. Li, X.-J. Ning, Performance of YSZ electrolyte layer deposited by atmospheric plasma spraying for cermet-supported tubular SOFC, Vacuum. 73 (2004) 699–703. doi:10.1016/j.vacuum.2003.12.096.

[25] S.P. Simner, J.P. Shelton, M.D. Anderson, J.W. Stevenson, Interaction between $La(Sr)FeO_3$ SOFC cathode and YSZ electrolyte, Solid State Ionics. 161 (2003) 11–18. doi:10.1016/S0167-2738(03)00158-9.

[26] J.-H. Lee, B.-K. Kim, K.-L. Lee, H.-I. Kim, K.-W. Han, A new catalyst monitoring sensor for gasoline engine using YSZ-Al_2O_3 as solid electrolyte and gas diffusion barrier, Sensors Actuators, B Chem. 59 (1999) 9–15.

[27] S. Fischer, R. Pohle, B. Farber, R. Proch, J. Kaniuk, M. Fleischer, R. Moos, Method for detection of NO_x

in exhaust gases by pulsed discharge measurements using standard zirconia-based lambda sensors, Sensors Actuators, B Chem. 147 (2010) 780–785. doi:10.1016/j.snb.2010.03.092.

[28] R. Ramamoorthy, P.K. Dutta, S.A. Akbar, Oxygen sensors: Materials, methods, designs and applications, J. Mater. Sci. 38 (2003) 4271–4282. doi:10.1023/A:1026370729205.

[29] X.J. Chen, K.A. Khor, S.H. Chan, L.G. Yu, Influence of microstructure on the ionic conductivity of yttria-stabilized zirconia electrolyte, Mater. Sci. Eng. A. 335 (2002) 246–252. doi:10.1016/S0921-5093(01)01935-9.

[30] V.G. Artemov, I.E. Kuritsyna, S.P. Lebedev, G.A. Komandin, P.O. Kapralov, I.E. Spektor, V.V Kharton, S.I. Bredikhin, A.A. Volkov, Analysis of electric properties of ZrO_2-Y_2O_3 single crystals using teraherz IR and impedance spectroscopy techniques, Russ. J. Electrochem. 50 (2014) 690–693. doi:10.1134/S1023193514070039.

[31] S. Cheng, M. Søgaard, L. Han, W. Zhang, M. Chen, A. Kaiser, P.V. Hendriksen, A novel CO_2 - and SO_2 -tolerant dual phase composite membrane for oxygen separation, Chem. Commun. 51 (2015) 7140–7143. doi:10.1039/C5CC00001G.

[32] L. Han, D. V. Christensen, A. Bhowmik, S.B. Simonsen, L.T. Hung, E. Abdellahi, Y.Z. Chen, N.V. Nong, S. Linderoth, N. Pryds, Scandium-doped zinc cadmium oxide as a new stable n-type oxide thermoelectric material, J. Mater. Chem. A. 4 (2016) 12221–12231. doi:10.1039/C6TA03126A.

[33] L. Han, N. Van Nong, L.T. Hung, T. Holgate, N. Pryds, M. Ohtaki, S. Linderoth, The influence of α- and γ-Al_2O_3 phases on the thermoelectric properties of Al-doped ZnO, J. Alloys Compd. 555 (2013) 291–296. doi:10.1016/j.jallcom.2012.12.091.

[34] L. Han, L.T. Hung, N. Van Nong, N. Pryds, S. Linderoth, The influence of spark plasma sintering temperature on the microstructure and thermoelectric properties of Al,Ga dual-doped ZnO, J. Electron. Mater. 42 (2013) 1573–1581. doi:10.1007/s11664-012-2325-x.

[35] P.H. Miller, The Electrical Conductivity of Zinc Oxide, Phys. Rev. 60 (1941) 890–895. doi:10.1103/PhysRev.60.890.

[36] S.Y. Kuo, W.C. Chen, F.I. Lai, C.P. Cheng, H.C. Kuo, S.C. Wang, W.F. Hsieh, Effects of doping concentration and annealing temperature on properties of highly-oriented Al-doped ZnO films, J. Cryst. Growth. 287 (2006) 78–84. doi:10.1016/j.jcrysgro.2005.10.047.

[37] V. Fathollahi, M.M. Amini, Sol–gel preparation of highly oriented gallium-doped zinc oxide thin films, Mater. Lett. 50 (2001) 235–239. doi:10.1016/S0167-577X(01)00231-2.

[38] T. Minami, Transparent conducting oxide semiconductors for transparent electrodes, Semicond. Sci. Technol. 20 S35 Semicond. Sci. Technol. 20 (2005) 35–44. doi:10.1088/0268-1242/20/4/004.

[39] S. Pirou, J. Gurauskis, V. Gil, M. Søgaard, P.V. Hendriksen, A. Kaiser, S. Ovtar, R. Kiebach, Oxygen permeation flux through 10Sc1YSZ-$MnCo_2O_4$ asymmetric membranes prepared by two-step sintering, Fuel Process. Technol. 152 (2016) 192–199. doi:10.1016/j.fuproc.2016.06.019.

[40] A.J. Samson, M. Søgaard, P.V. Hendriksen, (Ce,Gd)$O_{2-\delta}$-based dual phase membranes for oxygen separation, J. Memb. Sci. 470 (2014) 178–188. doi:10.1016/j.memsci.2014.07.028.

[41] K.A. Nielsen, M. Solvang, S.B.L. Nielsen, A.R. Dinesen, D. Beeaff, P.H. Larsen, Glass composite seals

for SOFC application, J. Eur. Ceram. Soc. 27 (2007) 1817–1822. doi:10.1016/j.jeurceramsoc.2006.05.046.

[42] K. Nakamoto, Infared and Raman Spectra of Inorganic and Coordination Compounds: Part A: Theory and Applications in Inorganic Chemistry, Sixth Edition, 2008. doi:10.1002/9780470405840.

[43] E. Turianicová, A. Obut, A. Zorkovská, P. Baláž, M. Matik, J. Briančin, The effects of LiOH and NaOH on the carbonation of $SrSO_4$ by dry high-energy milling, Miner. Eng. 49 (2013) 98–102. doi:10.1016/j.mineng.2013.05.017.

[44] M.E. Böttcher, P. Gehlken, Á. Fernández-González, M. Prieto, Characterization of synthetic $BaCO_3$ - $SrCO_3$ (witherite-strontianite) solid-solutions by Fourier transform infrared spectroscopy, Eur. J. Miner. 9 (1997) 519–528. doi:10.1127/ejm/9/3/0519.

[45] A. Periasamy, S. Muruganand, M. Palaniswamy, Vibrational studies of Na_2SO_4, K_2SO_4, $NaHSO_4$ and $KHSO_4$ crystals, J. Chem. 2 (2009) 981–989.

[46] J.M. Bermudez, J. García-Fayos, T.R. Reina, G. Reed, M. Milan, J.M. Serra, Thermochemical stability of $NiFe_2O_4$-$Ce_{0.8}Tb_{0.2}O_{2-\delta}$ under real conditions for its application in 4-end module oxygen transport membranes for oxycombustion, in: 14th Int. Conf. Inorg. Membr., Atlanta (USA), 2016.

[47] D. Bérardan, C. Byl, N. Dragoe, Influence of the preparation conditions on the thermoelectric properties of Al-doped ZnO, J. Am. Ceram. Soc. 93 (2010) 2352–2358. doi:10.1111/j.1551-2916.2010.03751.x.

[48] A. Janotti, C. Van de Walle, Fundamentals of zinc oxide as a semiconductor, Reports Prog. Phys. 72 (2009) 126501. doi:10.1088/0034-4885/72/12/126501.

Supporting Information

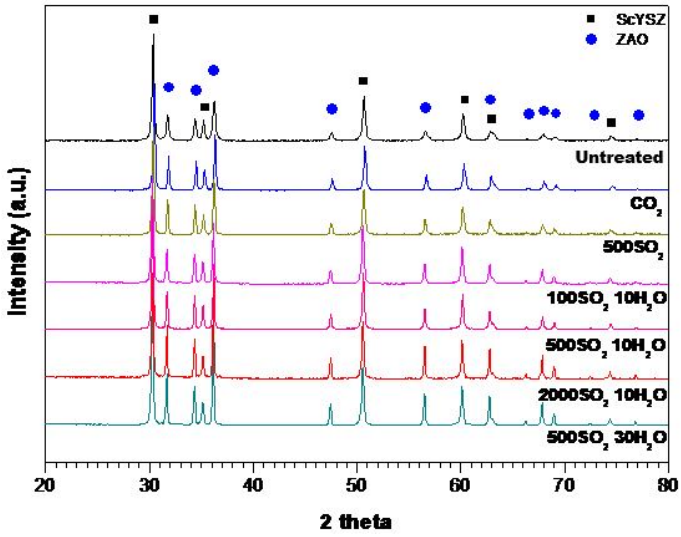

Figure 11: Powder XRD patterns of 10Sc1YSZ-AZO after treatment in different CO_2 and SO_2 atmospheres: untreated (black); in pure CO_2 (blue); in 500 ppm of SO_2 in CO_2 (yellow); in 100 ppm of SO_2 in CO_2 and 10% of steam (magenta); in 500 ppm of SO_2 in CO_2 and 10% of steam (pink); in 2000 ppm of SO_2 in CO_2 and 10% of steam (red) and in 500 ppm of SO_2 in CO_2 and 30% of steam (cyan).

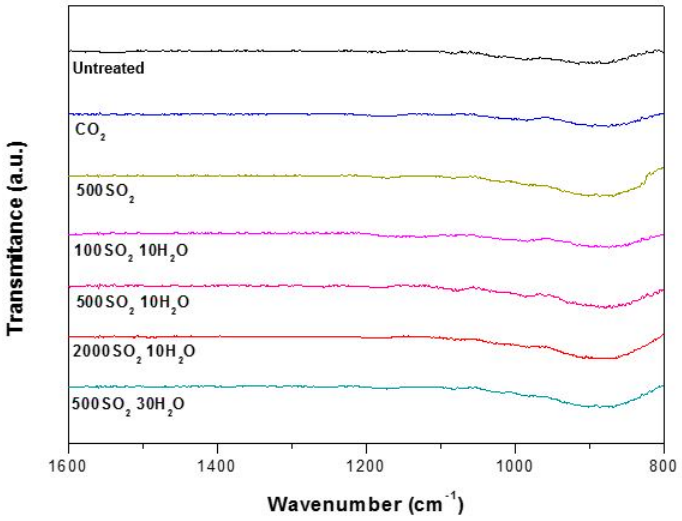

Figure 12: ATR-FTIR spectra of 10Sc1YSZ-AZO powders after treatment in different CO_2 and SO_2 atmospheres: untreated (black); in pure CO_2 (blue); in 500 ppm of SO_2 in CO_2 (yellow); in 100 ppm of SO_2 in CO_2 and 10% of steam (magenta); in 500 ppm of SO_2 in CO_2 and 10% of steam (pink); in 2000 ppm of SO_2 in CO_2 and 10% of steam (red) and in 500 ppm of SO_2 in CO_2 and 30% of steam (cyan).

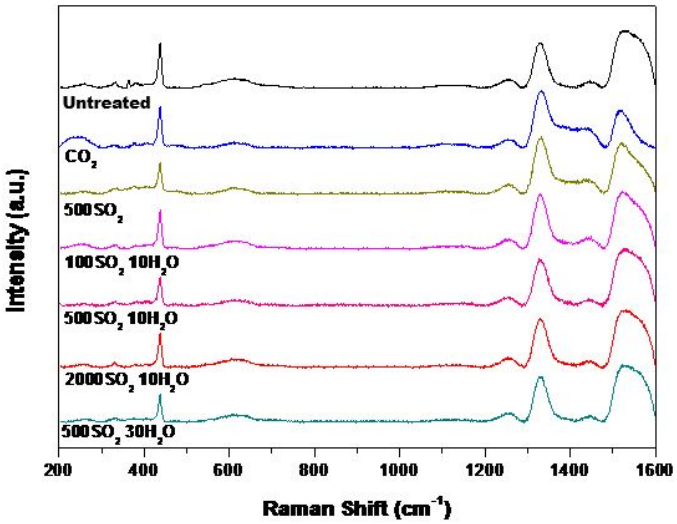

Figure 13: Raman spectra of10Sc1YSZ-AZO powder after treatment in different CO_2 and SO_2 atmospheres: untreated (black); in pure CO_2 (blue); in 500 ppm of SO_2 in CO_2 (yellow); in 100 ppm of SO_2 in CO_2 and 10% of steam (magenta); in 500 ppm of SO_2 in CO_2 and 10% of steam (pink); in 2000 ppm of SO_2 in CO_2 and 10% of steam (red) and in 500 ppm of SO_2 in CO_2 and 30% of steam (cyan).

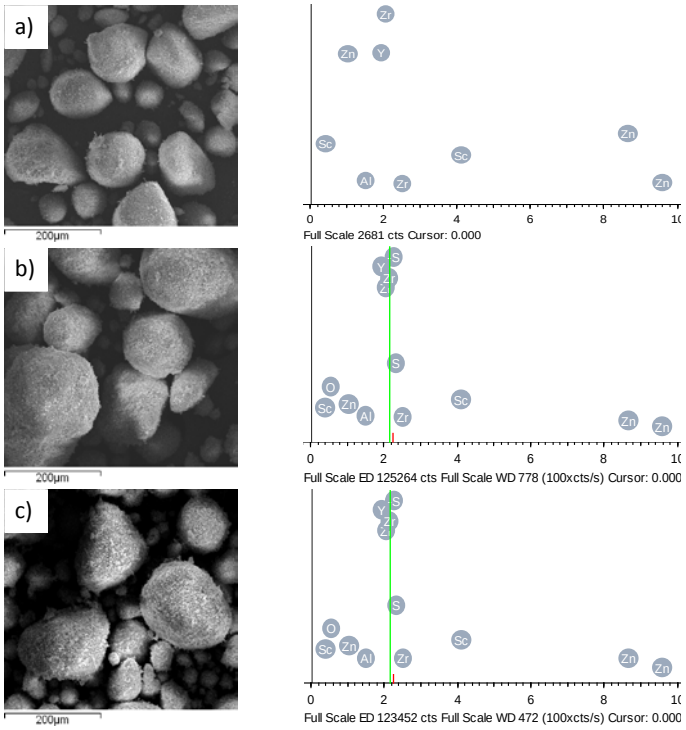

Figure 14: SEM pictures (left) and EDS/WDS spectra (right) of 10Sc1YSZ-AZO powder: a) untreated; b) after treatment in 2000 ppm of SO_2 in CO_2 and 10% of steam; and c) after treatment in 500 ppm of SO_2 in CO_2 and 30% of steam. For the treated samples, the results of the WDS are overlaying the EDS spectra (with a different scale). The red line represents the location of the sulphur signal, whereas the green line represents the signal of the background.